The within-subject application of diffusion tensor MRI and CLARITY reveals brain structural changes in *Nrxn2* deletion mice

Eleftheria Pervolaraki Ph.D[1]*, Adam L. Tyson MRes[2,3,4]*, Francesca Pibiri Ph.D[5], Steven L. Poulter Ph.D[5], Amy C. Reichelt Ph.D[6], R. John Rodgers Ph.D[7], Steven J. Clapcote Ph.D[1], Colin Lever Ph.D[5], Laura C. Andreae MBBS Ph.D[2,3]*, James Dachtler Ph.D[1,5]*

[1]School of Biomedical Sciences, University of Leeds, LS2 9JT, UK

[2]Centre for Developmental Neurobiology, Institute of Psychiatry, Psychology and Neuroscience, King's College London, London SE1 1UL, UK

[3]MRC Centre for Neurodevelopmental Disorders, King's College London, London SE1 1UL, UK

[4]Department of Forensic and Neurodevelopmental Sciences, Institute of Psychiatry, Psychology and Neuroscience, King's College London, London SE5 8AF, UK

[5]Department of Psychology, Durham University, South Road, Durham, DH1 3LE, UK

[6]Robarts Research Institute, Western University, London, Ontario, Canada, N6A 5B7, Canada

[7]School of Psychology, University of Leeds, LS2 9JT, UK

*These authors contributed equally.

Address for Correspondence: Dr J Dachtler, Department of Psychology, Durham University, South Road, Durham, DH1 3LE, UK. Email: james.dachtler@durham.ac.uk

Abstract

Background

Of the many genetic mutations known to increase the risk of autism spectrum disorder, a large proportion cluster upon synaptic proteins. One such family of presynaptic proteins are the neurexins (NRXN), and recent genetic and mouse evidence has suggested a causative role for *NRXN2* in generating altered social behaviours. Autism has been conceptualised as a disorder of atypical connectivity, yet how single-gene mutations affect such connectivity remains under-explored. To attempt to address this, we have developed a quantitative analysis of microstructure and connectivity leveraging diffusion tensor MRI (DTI) with high-resolution 3D imaging in optically cleared (CLARITY) brain tissue in the same mouse, applied here to the *Nrxn2α* knockout (KO) model.

Methods

Fixed brains of *Nrxn2α* KO mice underwent DTI using 9.4T MRI, and diffusion properties of socially-relevant brain regions were quantified. The same tissue was then subjected to CLARITY to immunolabel axons and cell bodies, which were also quantified.

Results DTI revealed decreases in fractional anisotropy and increases in apparent diffusion coefficient in the amygdala (including the basolateral nuclei), the anterior cingulate cortex, the orbitofrontal cortex and the hippocampus. Radial diffusivity of the anterior cingulate cortex and orbitofrontal cortex was significantly increased in *Nrxn2α* KO mice, as were tracts between the amygdala and the orbitofrontal cortex. Using CLARITY, we

find significantly altered axonal orientation in the amygdala, orbitofrontal cortex and the anterior cingulate cortex, which was unrelated to cell density.

Conclusions

Our findings demonstrate that deleting a single neurexin gene (*Nrxn2α*) induces atypical connectivity within socially-relevant brain regions. More generally, our combined within-subject DTI and CLARITY approach presents a new, more sensitive method of revealing hitherto undetectable differences in the autistic brain.

Key Words

MRI, CLARITY, social, autism, axons, diffusion, structure, imaging

Background

Autism is a common neurodevelopmental disorder, which is highly heritable (1). While heritability is high, it is also clear that autism is highly polygenic. Around ~400-1000 genes are involved in autism susceptibility (2-5). Many of these genes cluster upon proteins relating to synaptic signaling (6). A family of presynaptic proteins garnering recent interest have been the neurexins (*NRXNs*). NRXNs are encoded by three genes (*NRXN1, NRXN2, NRXN3;* note that *CNTNAP1* and *CNTNAP2* are sometimes referred to as *NRXN4*), of which two major isoforms exist: the longer α proteins with six laminin/neurexin/sex hormone (LNS) binding domains, and the shorter β proteins with one LNS binding domain (7, 8).

Mutations within all three *NRXN* genes have been linked to autism (6). Heterozygous deletions within *NRXN2* have been identified in a number of individuals with autistic phenotypes. These include an autistic boy and his father (who had severe language delay but not autism) who both had a frameshift mutation within exon 12 of *NRXN2* (9); a 570-kb de novo deletion of 24 genes at chromosome 11q13.1, including *NRXN2*, in a 21-year old man displaying a clinical phenotype including autistic traits (10); a 1.6Mb deletion at chromosome region 11q12.3-11q13.1, including *NRXN2*, in a 23-year old man with intellectual disability and behavioral problems (11); a de novo frameshift mutation identified in a Chinese man with autism spectrum disorder (ASD) (12), a 921 kb microdeletion at 11q13 in a 2 year old boy who had language and developmental delay (although did not meet the autism diagnosis criteria) (13) and a paternally inherited microRNA miR-873-5p variant in an ASD individual which altered binding affinity for several risk-genes including *NRXN2* and *CNTNAP2* (*NRXN4*) (14). Furthermore, recently, two large-scale reports have identified *NRXN2* with ASD risk. A study of 529 ASD patients and 1,923 controls in a Chinese population identified two *NRXN2* variants which significantly increase ASD risk (15). The second study employed machine learning approaches across 5000 ASD families to rank the importance of ASD candidate genes, and ranks *NRXN2* in the top ~0.5% of genes, i.e. 113th (16). For comparison, *NRXN1*, for which the evidence base for its links to ASD is broader and stronger, ranks 45, and *CNTNAP2* ranks 211th (16). Consistent with these association studies, we and others have previously found that homozygous or heterozygous deletion of *Nrxn2*α induces impairment in social approach and social recognition (17-19). In

summary, although mutations within *NRXN2* are rare, understanding how they may drive social, ASD-relevant behavioural changes is important. One important goal is to help elucidate how apparently convergent pathophysiology in ASD emerges despite marked genetic heterogeneity (Insert ref Geschwind & State, 2015 cited above); mapping brain alterations driven by different single genes is thus a crucial task.

Currently it is unknown whether deletion of *Nrxn2*α changes the brain's microstructure and connectivity. One previous study found coarse alterations to cell layer thickness within the hippocampus of *Nrxn2*α homozygous KOs (20). However, cell density measurements are unlikely to reveal the true extent of changes within the autistic brain. Within the current study, we have addressed this by developing a dual imaging approach (DTI and CLARITY) that quantifies the alignment and density of white matter, applied here to brain regions known to support social behavior in a mouse model of autism.

Diffusion tensor MRI (or DTI) is based upon the movement of water molecules, a measure that is termed fractional anisotropy (FA). Apparent diffusion coefficient (ADC) is similar to FA, but quantifies diffusion restriction as opposed to the spatial symmetry of diffusion. This approach has been used to explore neuropathological markers in autistic patients; alterations in myelination, axonal abundance, size and orientation all modify FA and ADC values (21-23). Using the preferred direction of the diffusion of tensors between brain regions can be used to explore their potential connection. Quantification of those computed streamlines by FA and axial and/or radial

diffusion can indicate impairments in regional connectivity. Since aberrant brain connectivity is likely a core feature of autism (24), we reasoned that the candidate method for probing the autistic brain should combine tractographic techniques. Accordingly, here, we combined high resolution imaging of labelled neuronal tracts in brains rendered transparent by CLARITY with DTI.

CLARITY is a recent development that renders tissue optically transparent and macromolecule permeable (25). This permits antibody staining and imaging of much larger tissue volumes than possible under traditional immunofluorescence techniques. By examining fiber orientation without sectioning-related artefacts and biases, axonal staining in cleared tissue affords a deeper understanding of the microstructure and connectivity of a brain region.

Given the social impairments found within *Nrxn2α* mice, we sought to examine those brain regions most closely linked with social behavior (See Supplemental Materials). Briefly, we identified four regions of interest (ROIs): the amygdala, and three brain regions strongly and directly connected to the amygdala; the hippocampus, orbitofrontal cortex (OFC), and anterior cingulate cortex (ACC). As predicted, connectivity was abnormal in *Nrxn2α* mice.

Methods

Ethics

All procedures were approved by the University of Leeds and Durham University Animal Ethical and Welfare Review Boards and were performed

under UK Home Office Project and Personal Licenses in accordance with the Animals (Scientific Procedures) Act 1986.

Animals

Full details of the animals, their background, genotyping and housing can be found elsewhere (17). In brief, male B6;129-*Nrxn3tm1Sud*/*Nrxn1tm1Sud*/*Nrxn2tm1Sud*/J mice (JAX #006377) were purchased from the Jackson Laboratory and outbred once to the C57BL/6NCrl strain (Charles River, Margate, United Kingdom) to obtain mice that were individually Nrxn2α KO heterozygotes. Subsequently, HET knockout males were bred with HET females (cousin mating).

Experimental animals

6 adult wild-type males (Charles River, Margate, UK) and 6 age matched littermate Nrxn2α KO homozygotes (71 days ± 6 days old (SEM)) were perfused-fixed with 4% paraformaldehyde (PFA) in 0.1 M phosphate buffer saline (PBS) and the brains extracted. The brains were immersed in 4% PFA/0.1 M PBS for a minimum of 48 hours prior to imaging. During imaging, the samples were placed in custom-built MR-compatible tubes containing Fomblin Y (Sigma, Poole, Dorset, UK).

Due to the relatively low variance, and owing to the complexity and methodological nature in our experimental approach, we achieved significance by groups of 6 (power provided in Results). No data was

177 excluded from the study. Sample randomisation was performed by JD, with
178 experimenters (EP and ALT) blinded to genotype.
179
180 **Data Acquisition**
181 Image acquisition has been described elsewhere (26). Each brain was 3D
182 imaged using the protocol TE: 35 ms, TR: 700 ms and 10 signal averages.
183 The field of view was set at 128 x 128 x 128, with a cubic resolution of 100
184 µm/pixel and a b value of 1200 s/mm^2. Further details can be found in
185 Supplemental Materials.
186
187 **Regions of Interest**
188 Our DTI approach was to undertake an *a posteriori* analysis of neural
189 organization in regions of interest (ROIs) identified by previous literature as
190 socially-relevant (see Supplemental Materials). We identified a canonical
191 coronal slice (100 µm) for a given ROI from the standard mouse brain atlas
192 (Figure 1A-D) (27). We analysed three coronal slices centred on the canonical
193 slice, totalling 300 µm in anterior/posterior extent.
194
195 **CLARITY**
196 Following MR imaging, the brains were washed in PBS to remove all Fomblin
197 Y and then incubated for 7 days in hydrogel solution at 4°C prior to
198 polymerisation at 37°C for 3.5 hours. The tissue was cut into 1.5 mm coronal
199 sections using a custom 3D-printed brain-slicing matrix based on MRI scans
200 of an adult C57BL/6 mouse brain (28) and incubated in clearing buffer for 24
201 days at 37°C with shaking. The cleared tissue was then washed in PBSTN3

(0.1% TritonX-100 and 1.5mM sodium azide in PBS) for 24 hours at room temperature and incubated in primary antibody solution (neurofilament (Aves NF-H) 1:100 in $PBSTN_3$) at 37°C with shaking for 13 days. Samples were washed, and then incubated in secondary antibody (AlexaFluor 488 goat anti-chicken IgY) as per the primary. Sections were washed again, and incubated in 3.6 µM DAPI (4',6-diamidino-2-phenylindole) followed by 85% glycerol in PBS for refractive index matching.

Cleared samples were imaged using a Zeiss 7MP multiphoton microscope at 770nm using a 20x objective lens (W Plan-Apochromat, NA 1.0, WD 1.7mm). Images (512 x 512 x 512 voxels or 265 x 265 x 265 µm with an isotropic resolution of 520 nm) were acquired in ACC, basolateral (BLA) and basomedial amygdala and OFC) in both hemispheres. DAPI and neurofilament signal was segmented into cell nuclei and axons, and the resulting binary images were used to generate values for cell density, axonal density and axonal alignment.

Full CLARITY methodological details are available within Supplemental Materials.

Data Availability

Codes to analyse CLARITY datasets are made available by author LCA by email request to either JD or LCA, subject to reference to the current paper. The datasets used and/or analysed during the current study are available from the corresponding author on reasonable request.

Data Analysis

All data are expressed as mean ± standard error of the mean (SEM). To assess the variance between genotypes within a single brain structure across hemispheres (given the importance of hemispheric differences in ASD (29)), data was analyzed by within subject repeated measures two-way ANOVAs, with Sidak multiple corrections employed on post hoc testing, or unpaired T-tests. To correct for multiple comparisons, we employed the Benjamini-Hochberg Procedure (corrected P values stated). Non-significant statistical results, particularly hemisphere comparisons, can be found in Supplemental Materials. Statistical testing and graphs were made using GraphPad Prism version 6 and SPSS v22.

Results

Nrxn2α deletion disrupts DTI measures of microstructure in social brain regions

To assess whether *Nrxn2α* deletion alters gross morphology, we quantified whole brain volume using DTI. We found total brain volume for wild-types and *Nrxn2α* KOs was similar (456.0 ± 14.76 vs. 466.2 ± 11.0 mm^3 (respectively); $t_{(10)} = 0.55$, $p = 0.59$). Thus, Nrxn2α deletion does not change total brain size.

To quantitatively measure DTI, we examined FA and ADC. FA analyses changes in the linear orientation (i.e. along an axonal tract), whereas ADC (mean diffusivity) averages diffusion in all directions (i.e. the X, Y and Z axis), which is sensitive to changes such as altered alignment. The amygdala is

critically important for social behaviours. To assess whether amygdalar alterations might account for social impairments in Nrxn2α KO mice, we segmented the whole amygdala structure and the basolateral nuclei along the anterior-posterior axis.

The posterior amygdala showed a significant reduction in FA in *Nrxn2α* KO mice (Figure 2A-B) (anterior: genotype ($F_{(1, 10)} = 5.81$, $p = 0.056$); posterior: genotype ($F_{(1, 10)} = 11.2$, $p = 0.025$, power = 85.4%)). This FA reduction was also observed specifically in the BLA, a region strongly associated with social behaviours (Figure 2C; genotype ($F_{(1, 10)} = 6.31$, $p = 0.049$, power = 62.1%)). ADC was not significantly altered in the anterior amygdala, posterior amygdala or BLA (Figure 2D-F; all genotype: $F_{(1, 10)} < 1$).

We conducted the same analysis for the two prefrontal regions implicated in social behaviour and autism: the OFC and ACC. The pattern of results was similar for both regions: FA was not altered, while ADC was increased in the OFC (Figure 3A-B) and the ACC (Figure 3C-D). FA for the OFC was not significantly altered (genotype: ($F_{(1, 10)} = 3.04$, $p = 0.079$)) but ADC was significantly increased (genotype: ($F_{(1, 10)} = 8.20$, $p = 0.043$, power = 73.3%)). The ACC was unaltered in FA ($t_{(10)} = 1.70$, $p = 0.08$) but had significantly increased ADC ($t_{(10)} = 7.52$, $p = 0.002$, power = 99.9%).

We sought to examine whether changes in the amygdala (Supp. Figure 3), OFC or ACC FA and ADC were driven by diffusion in the primary axis (λ_1) or the radial orientations (λ_2 and λ_3) by characterisation of AD (primary) and RD

(radial). Within the OFC (Figure 3E-F), AD was significantly increased (genotype: ($F_{(1, 10)}$ = 10.74, p = 0.029, power = 83.9%)), as was RD (genotype: ($F_{(1, 10)}$ = 18.26, p = 0.009, power = 97.0%)), suggesting that both along-tract diffusion and tract branching were affected. However, in the ACC (Figure 3G-H), only RD was significantly increased ($t_{(10)}$ = 5.65, p = 0.007, power = 99.9%), with no alteration in AD ($t_{(10)}$ = 1.69, p = 0.09). Increased RD is thought to reflect demyelination or changes in axonal density or orientation (30).

DTI reveals altered hippocampal microstructure in *Nrxn2α* KO mice

The hippocampus has recently been associated with social motivation and social recognition. Since the specific contributions of the dorsal and ventral hippocampal poles remain unclear, we segmented the whole hippocampus into anterior (Bregma -1.94 mm), middle (Bregma -2.46 mm) (both dorsal) and posterior (Bregma -3.28 mm) (incorporating ventral regions) levels.

FA values in the anterior, mid and posterior hippocampus were not significantly altered (see Supp. Table 1 for statistics and Supp. Figure 4A-C). Similarly, ADC was unaltered for the anterior and mid hippocampus (Supp. Table 1 for statistics and Supp. Figure 4D-E), but was significantly increased in *Nrxn2α* KO mice in the posterior hippocampus (genotype: ($F_{(1, 10)}$ = 8.80, p = 0.036, power = 76.6%); Supp. Figure 4F). There were no significant genotype differences in AD in any of the hippocampal regions (Supp. Figure 5A-C). However, RD was significantly increased in the posterior hippocampus in *Nrxn2α* KO mice (genotype: ($F_{(1, 10)}$ = 10.83, p = 0.027, power = 84.2%;

Supp. Figure 5F) but not in anterior and mid regions (see Supp. Table 1; Supp. Figure 5D-E). In summary, the microstructural measures most altered by *Nrxn2α* deletion were increases in ADC and RD, and both these alterations occurred in the posterior hippocampus, in line with recent work suggesting a role for ventral hippocampus in social memory (31).

DTI tractography reveals *Nrxn2α* deletion affects connectivity between the amygdala and orbitofrontal cortex

The amygdala is strongly and bidirectionally connected to both the hippocampus (32) and the OFC (33). As all three regions are themselves important for social behaviour, and autism is thought to be related to abnormal connectivity (24), we performed tractography analysis between the amygdala (and specifically the BLA) and the hippocampus, and between the amygdala and the OFC.

From the anterior amygdala, we examined the diffusivity (AD and RD) of connections to the anterior and posterior hippocampus (Supp. Figure 6). We did not observe differences in RD in the tracts connecting the amygdala with the hippocampus (see Supp. Table 2 for non-significant statistics). Although AD between the anterior amygdala and anterior hippocampus did not differ by genotype, there was a significant interaction between genotype and hemisphere (genotype x hemisphere ($F_{(1,\ 10)}$ = 12.12, p = 0.023, power = 88.0%; Figure 4A); post hoc analysis shows this was driven by larger right-vs-left hemisphere AD values within the *Nrxn2α* KOs only (p = 0.012). This difference could be driven by the BLA; there was increased AD in both the

BLA/anterior hippocampus tracts (genotype x hemisphere ($F_{(1, 10)}$ = 10.53, p = 0.032, power = 83.2%) and the BLA/posterior hippocampus tracts (genotype x hemisphere ($F_{(1, 10)}$ = 12.97, p = 0.020, power = 90%), which again was related to larger right-vs-left hemisphere values in the *Nrxn2α* KOs (BLA/anterior Hippocampus: p = 0.004 and BLA/posterior Hippocampus: p = 0.001, (Figure 4C-D)) but not the wild-type (anterior: p = 0.87; posterior:p = 1.00). These results indicate that there are differences for the connectivity of the amygdala with the hippocampus within the left and right hemisphere in *Nrxn2α* KO mice, with increased axial diffusivity in the right hemisphere. This finding is particularly interesting, as hemispheric differences in functional connectivity, particularly affecting connections from the right amygdala, have been found children with ASD (34, 35).

Finally, we tested connections between the amygdala and the orbitofrontal cortex. For AD, wild-type and Nrxn2α KO mice did not differ by genotype (Figure 4E: genotype: ($F_{(1, 10)}$ = 2.85, p = 0.09), hemisphere: ($F_{(1, 10)}$ = 6.38, p = 0.052). RD was strikingly higher in *Nrxn2α* KO mice (Figure 4F: genotype: ($F_{(1, 10)}$ = 26.06, p = 0.023, power = 99.5%)), indicative of a change in demyelination, axonal density or orientation (30).

CLARITY reveals fibre disruption in *Nrxn2α* KO mice in the amygdala, orbitofrontal cortex, and anterior cingulate cortex

To further explore the differences as revealed by DTI, we performed CLARITY on the same brain tissue used in DTI, and stained with neurofilament and DAPI to label axons and cell bodies, respectively. We were then able to derive

both the axonal alignment (as in, the geometric alignment of axons (from linear alignment to random) within 3D space (see Supp. Figure 2)) and density of the stained fibers, in addition to the cell density.

The pattern of results was broadly similar for both the prefrontal cortical ROIs. That is, first, axonal alignment was increased in *Nrxn2α* KO mice in the ACC (Figure 5D: genotype: ($F_{(1, 10)}$ = 16.06, p = 0.011, power = 94.9%) but not the OFC (Figure 5G: genotype: ($F_{(1, 10)}$ = 5.56, p = 0.059). Second, this could not be explained by a difference in cell density, since that was similar between the KO and wild-type mice in both the ACC (Figure 5F: genotype: ($F_{(1, 10)}$ <1), hemisphere: ($F_{(1, 10)}$ = 1.73, p = 0.11) and the OFC (Figure 5H: genotype: ($F_{(1, 10)}$ = 3.09, p = 0.08). An increase in axonal density in *Nrxn2α* KO mice was reliable in the ACC (Figure 5E: genotype: ($F_{(1, 10)}$ = 14.64, p = 0.014, power = 93.0%), but not in the OFC (Figure 5H: genotype: ($F_{(1, 10)}$ = 3.09, p = 0.083).

We further examined two regions of the anterior amygdala, the BLA and basomedial (BMA) nuclei, where altered social cellular responses have been reported in human autism (36). We did not observe any significant differences for axonal alignment or fibre density in the BLA (see Supp. Figure 7A-C), but whereas axonal alignment (Figure 5J, genotype: $F_{(1, 10)}$ = 7.70, p = 0.045, power = 70.6%) but not axonal density (Figure 5K: genotype: ($F_{(1, 10)}$ = 6.10, p = 0.054) was increased in *Nrxn2α* KO mice in the basomedial nuclei, while cell density was unaffected (Figure 5L: genotype: ($F_{(1, 10)}$ <1). Alterations in axonal alignment and density as directly revealed by CLARITY could explain

the increases in diffusivity and RD in the prefrontal regions, as measured by DTI.

To test the specificity of these alterations, we examined three further brain regions; the primary motor cortex (M1; Supp. Figure 7D-F), the primary somatosensory cortex (S1; Supp. Figure 7H-J) and the barrel field (BF; Supp. Figure 7K-M). Interestingly, although there were differences between the hemispheres, there were no statistical differences between the genotypes or genotype x hemisphere interactions for any measure (Supp. Table 3), suggesting some specificity of the alterations in social-relevant brain regions in *Nrxn2α* KO mice.

In summary, in both the prefrontal ROIs, namely the OFC, and the ACC, DTI showed that ADC and RD were increased in *Nrxn2α* KO mice, likely related to complementary analysis from CLARITY showing that axonal alignment was altered in *Nrxn2α* KO mice in both prefrontal ROIs.

Discussion

Interestingly, the single-gene deletion of *Nrxn2α* captures several key aspects of human ASD. In terms of behaviour, three studies have now found social deficits associated with *Nrxn2α* KO (17-19); in terms of brain structure, as reported here (summarised below), the *Nrxn2α* KO mouse model shows altered microstructure and connectivity patterns in socially-relevant brain regions reminiscent of changes in ASD.

A DTI approach has been used for some time to explore neuropathological markers in autistic patients; alterations in myelination, axonal abundance, size and orientation all modify FA and ADC values (21, 37), specifically by reducing amygdala FA (23, 37), and have been used as a quantitative measure of changes to brain white matter integrity (23, 24). Increased cortical ADC typically indexes reduced functionality: e.g. increased hippocampal ADC is associated with mild cognitive impairment (38, 39) and predicts verbal and visuospatial memory in old healthy controls (40). Furthermore, both increased RD of various white matter tracts (41, 42) and increased whole-brain AD (42) have been observed in ASD. The *Nrxn2α* KO mouse reproduces many of these specific changes, including reduced FA and increases in ADC, AD and RD. Whole brain increases in ADC, AD and RD (but not FA) have been reported in ASD children, as have increases in ADC and RD in frontal cortex tracts (42). This is in agreement with other studies noting increased ADC in frontal cortex in ASD (37), as we observed here in both the prefrontal regions examined, the OFC and ACC. Likewise, FA was reduced in the amygdala in ASD children and adolescents (43), and right-sided lateralisation of abnormal amygdala/hippocampus-related connections, as seen in our *Nrxn2α* KO mouse, has been noted in high-functioning adolescents/adults with autism (44).

Our findings corroborate these quantifications of clinical autism, but highlights the question of what do the different measures of ADC, FA, AD and RD represent? Importantly, we observed these microstructural changes in various socially-relevant brain regions against a background of unchanged cell

density in all our study's ROIs. Unexpectedly, this highlights the power of our new approach. Dudanova et al. (2007) concluded from measures of cell counting and cortical cell layer thickness that NRXN2 played little role in normal brain development (20). Indeed, in earlier studies, it was suggested that deletion of all *Nrxns* was unlikely to affect synaptic development but instead disrupts synaptic function (45). We propose that measures such as two-dimensional cell counting may be underestimating the impact of genetic mutations upon normal development. By staining cleared brain tissue with a nuclear marker and performing automated three-dimensional cell counting, we found no effect of *Nrxn2α* deletion on cell density in any region of interest examined. But this belies the clear effects upon microstructure integrity across multiple regions as measured by both DTI and CLARITY, and its specificity; only the socially-relevant brain regions we tested were disrupted, and not primary sensory or motor regions. Future studies will benefit from employing more sensitive measures of brain structure and connectivity to determine the relevance of genetic mutations in development.

FA and ADC can be influenced by changes in axonal density and alignment (e.g. by myelination, demyelination, axonal damage, loss of white matter coherence (46)). It is likely that the axonal alignment metric used to quantify CLARITY more closely reflects the ADC measure of DTI, given that ADC (or mean diffusivity) equally weights diffusion across all eigenvectors and does not bias the primary eigenvector as FA does. Thus, it is likely that alterations in the properties of axons in Nrxn2α KO mice are driving these changes in FA and ADC. Given we mostly see differences in RD, thought to reflect tract

branching and myelination (as it measures λ_2 and λ_3), it is possible that the orientation in the perpendicular not parallel orientation of fibres is mostly affected. Given the differences in the amygdala, OFC and ACC, it is possible that even though neuronal densities are similar in the Nrxn2α KO brain, it is the connections between neurones and brain regions that are perturbed. This would be consistent with the idea that connectivity disruption may represent a core feature of autism (47). A broader question is how does the loss of *Nrxn2α* account for changes in axonal organisation? Ultimately, this question requires further studies. Others have shown that in Nrxn2α KO mice, excitatory transmitter release is reduced, as is short-term plasticity (18). Reduced glutamatergic release, even at a relatively long range to the synapse, can change the complexity of dendritic arbors (48). As this is a gene deletion model, it is conceivable that altered glutamatergic signalling during early development impairs appropriate synapse maturation, leading to the structural changes we see herein. Further, how or whether these structural changes fully explain the social impairments of Nrxn2α KO mice would require new studies. Conceivably, inducible knock-down of Nrxn2 (by inducible knockout, siRNA, optogenetics etc.) within a specific brain region would provide evidence that social abnormalities are being driven by Nrxn2 loss. However, developmentally-dependent altered connectivity would be harder to definitively manipulate to explain changes in social behaviours.

Here we have developed a new application of CLARITY to quantitatively investigate disease models by combining DTI with high resolution 3D imaging and automated analysis of axonal fibres in a within subject study. Inevitably,

there are some technical limitations that will require future refinement as this technology matures.

First, while we used CLARITY and immunolabeling to identify axons, we cannot know whether axon-related changes alone reflect all the changes we observed for our DTI measures. Second, whilst we can segment entire brain regions for DTI analysis, it was not practical to image larger brain areas at the necessary resolution for CLARITY. While it is theoretically possible that we may bias sampling of each brain region by picking ROIs for multiphoton imaging, this was done using atlas-defined coordinates and by an experimenter blind to the DTI results, so minimising any bias. However, within the current study, we were only able to apply the CLARITY approach to the amygdala, OFC and ACC. It was not practical to apply this methodology to the hippocampus, due to its extremely heterogeneous structure. The small cubic ROIs could not be reproducibly positioned, and larger ROIs to average across larger areas of the hippocampus were not possible. Although imaging of fibre tracts in large volumes of cleared tissue is possible (49), fluorescent labelling limitations make it impractical for a study of this nature. Despite this, as the adoption of the CLARITY technique increases, we hope that the use of DTI and CLARITY to study connectivity across spatial scales will become commonplace.

As yet, no one DTI protocol has emerged as the standard for *in vivo* or *ex vivo* imaging. Indeed, there has been debate regarding the best number of diffusion gradients to use, among other parameters (50). Whilst some claim a

minimum of 30 directions are required to estimate anisotropy (50), others claim that the benefits of using more than six are limited (51-54). A limitation of these studies is that these competing claims have not been complemented with standard neuroanatomical techniques. Our study provides further evidence that six directions are sufficient to detect genotypic differences. Where we found DTI differences, these were corroborated by the quantification of CLARITY (OFC, ACC, with BLA differences not reaching statistical significance after multiple-comparison correction). A further potential limitation of the current study is that groups of six animals may be underpowered. We argue for our approach here as follows. First, low variance in the datasets permits smaller group sizes. Second, for 18 of our 22 significant results, the observed power was more than 80%. Third, given the technical complexity of this approach, particularly in its early adoption and refinement stages, large sample throughput of multiple brain regions is challenging.

In summary, our combined use of DTI and CLARITY has revealed changes in microstructure and connectivity of socially-relevant brain regions in *Nrxn2α* KO mice that may underlie their deficits in social behaviour. It is hard to conceive how these changes could have been observed using classical experimental approaches. We envisage this approach will deliver a new level of detail in the connectivity approaches to understanding autism.

Abbreviations

ACC: anterior cingulate cortex

AD: axial diffusivity

ADC: apparent diffusion coefficient

ASD: autism spectrum disorder

BLA: basolateral amygdala

CLARITY: optically cleared brain tissue

DTI: diffusion tensor imaging

FA: fractional anisotropy

OFC: orbitofrontal cortex

Nrxn2: neurexin II

RD: radial diffusivity

ROI: region of interest

Declarations

Ethics approval and consent to participate

All experiments were performed under UK Home Office Project and Personal Licenses in accordance with the Animals (Scientific Procedures) Act 1986, and with the approval of the University of Leeds and Durham University Animal Ethical and Welfare Review Boards.

Consent for publication

Not applicable

Availability of data and material

The codes used to quantify the CLARITY datasets are made available by author LCA by email request to authors LCA or JD, subject to reference to the

current paper. The datasets used and/or analysed during the current study are available from the corresponding author on reasonable request.

Competing interests

The authors declare no competing interests.

Funding

This work was supported by the Guy's and St. Thomas' Charity Prize PhD scholarship to ALT, a Medical Research Council (UK) grant (G0900625) to SJC and RJR, a University of Leeds Wellcome Trust ISSF (UK) Fellowship, a Royal Society (UK) grant (RG130316), an Alzheimer's Society Fellowship (AS-JF-15-008) to JD, a British Pharmacological Society (UK) grant to JD and CL, a BBSRC grant to LCA (BB/P000479/1) and a BBSRC grant to CL (BB/M008975/1). We acknowledge financial support from the Innovative Medicines Initiative Joint Undertaking under grant agreement no. 115300, resources of which are composed of financial contribution from the European Union's Seventh Framework Programme (FP7/2007–2013) and EFPIA companies' in kind contribution, the Mortimer D Sackler Foundation and the Sackler Institute for Translational Neurodevelopment (ALT and LCA). Some analysis scripts were provided to ALT at the Computational Image Analysis in Cellular and Developmental Biology course at the Marine Biological Laboratory (Woods Hole, MA, USA), funded by National Institutes of Health (R25 GM103792-01).

Authors' contribution

EP, ALT, LCA and JD conceived the study. EP and ALT performed the experiments. EP, ALT, LCA and JD analysed the data. SJC, RJR, LCA and JD funded the study. All authors contributed to writing the paper. All authors have read and approved the final manuscript.

Acknowledgements

Not applicable.

References

1. Sandin S, Lichtenstein P, Kuja-Halkola R, Larsson H, Hultman CM, Reichenberg A. The familial risk of autism. Jama. 2014;311(17):1770-7.
2. Cardno AG, Gottesman, II. Twin studies of schizophrenia: from bow-and-arrow concordances to star wars Mx and functional genomics. American journal of medical genetics. 2000;97(1):12-7.
3. Ronald A, Happe F, Bolton P, Butcher LM, Price TS, Wheelwright S, et al. Genetic heterogeneity between the three components of the autism spectrum: a twin study. Journal of the American Academy of Child and Adolescent Psychiatry. 2006;45(6):691-9.
4. Ronemus M, Iossifov I, Levy D, Wigler M. The role of de novo mutations in the genetics of autism spectrum disorders. Nature reviews Genetics. 2014;15(2):133-41.
5. Geschwind DH, State MW. Gene hunting in autism spectrum disorder: on the path to precision medicine. The Lancet Neurology. 2015;14(11):1109-20.
6. Sahin M, Sur M. Genes, circuits, and precision therapies for autism and related neurodevelopmental disorders. Science. 2015;350(6263).
7. Lise MF, El-Husseini A. The neuroligin and neurexin families: from structure to function at the synapse. Cellular and molecular life sciences : CMLS. 2006;63(16):1833-49.
8. Sudhof TC. Synaptic Neurexin Complexes: A Molecular Code for the Logic of Neural Circuits. Cell. 2017;171(4):745-69.
9. Gauthier J, Siddiqui TJ, Huashan P, Yokomaku D, Hamdan FF, Champagne N, et al. Truncating mutations in NRXN2 and NRXN1 in autism spectrum disorders and schizophrenia. Human genetics. 2011;130(4):563-73.
10. Mohrmann I, Gillessen-Kaesbach G, Siebert R, Caliebe A, Hellenbroich Y. A de novo 0.57 Mb microdeletion in chromosome 11q13.1 in a patient with speech problems, autistic traits, dysmorphic features and multiple endocrine neoplasia type 1. European journal of medical genetics. 2011;54(4):e461-4.
11. Boyle MI, Jespersgaard C, Nazaryan L, Ravn K, Brondum-Nielsen K, Bisgaard AM, et al. Deletion of 11q12.3-11q13.1 in a patient with intellectual disability and childhood facial features resembling Cornelia de Lange syndrome. Gene. 2015;572(1):130-4.

12. Li J, Wang L, Gou H, Shi L, Zhang K, Tang M, et al. Targeted sequencing and functional analysis reveal brain-size-related genes and their networks in autism spectrum disorders. Molecular Psychiatry. 2017;22:1282–90.
13. Yuan H, Li X, Wang Q, Yang W, Song J, Hu X, et al. A de novo 921Kb microdeletion at 11q13.1 including neurexin 2 in a boy with developmental delay, deficits in speech and language without autistic behaviors. European journal of medical genetics. 2018.
14. Williams SM, An JY, Edson J, Watts M, Murigneux V, Whitehouse AJO, et al. An integrative analysis of non-coding regulatory DNA variations associated with autism spectrum disorder. Molecular psychiatry. 2018.
15. Wang J, Gong J, Li L, Chen Y, Liu L, Gu H, et al. Neurexin gene family variants as risk factors for autism spectrum disorder. Autism research : official journal of the International Society for Autism Research. 2018;11(1):37-43.
16. Duda M, Zhang H, Li HD, Wall DP, Burmeister M, Guan Y. Brain-specific functional relationship networks inform autism spectrum disorder gene prediction. Translational psychiatry. 2018;8(1):56.
17. Dachtler J, Glasper J, Cohen RN, Ivorra JL, Swiffen DJ, Jackson AJ, et al. Deletion of alpha-neurexin II results in autism-related behaviors in mice. Translational psychiatry. 2014;4:e484.
18. Born G, Grayton HM, Langhorst H, Dudanova I, Rohlmann A, Woodward BW, et al. Genetic targeting of NRXN2 in mice unveils role in excitatory cortical synapse function and social behaviors. Frontiers in synaptic neuroscience. 2015;7:3.
19. Dachtler J, Ivorra JL, Rowland TE, Lever C, Rodgers RJ, Clapcote SJ. Heterozygous deletion of alpha-neurexin I or alpha-neurexin II results in behaviors relevant to autism and schizophrenia. Behavioral neuroscience. 2015;129(6):765-76.
20. Dudanova I, Tabuchi K, Rohlmann A, Sudhof TC, Missler M. Deletion of alpha-neurexins does not cause a major impairment of axonal pathfinding or synapse formation. The Journal of comparative neurology. 2007;502(2):261-74.
21. Beaulieu C. The basis of anisotropic water diffusion in the nervous system - a technical review. NMR in biomedicine. 2002;15(7-8):435-55.
22. Barnea-Goraly N, Kwon H, Menon V, Eliez S, Lotspeich L, Reiss AL. White matter structure in autism: preliminary evidence from diffusion tensor imaging. Biological psychiatry. 2004;55(3):323-6.
23. Noriuchi M, Kikuchi Y, Yoshiura T, Kira R, Shigeto H, Hara T, et al. Altered white matter fractional anisotropy and social impairment in children with autism spectrum disorder. Brain research. 2010;1362:141-9.
24. Belmonte MK, Allen G, Beckel-Mitchener A, Boulanger LM, Carper RA, Webb SJ. Autism and abnormal development of brain connectivity. The Journal of neuroscience : the official journal of the Society for Neuroscience. 2004;24(42):9228-31.
25. Chung K, Wallace J, Kim SY, Kalyanasundaram S, Andalman AS, Davidson TJ, et al. Structural and molecular interrogation of intact biological systems. Nature. 2013;497(7449):332-7.
26. Pervolaraki E, Anderson RA, Benson AP, Hayes-Gill B, Holden AV, Moore BJ, et al. Antenatal architecture and activity of the human heart. Interface focus. 2013;3(2):20120065.
27. Paxinos G, Franklin K. The Mouse Brain in Stereotaxic Coordinates. Third ed: Academic Press; 2008.

28. Tyson AL, Hilton ST, Andreae LC. Rapid, simple and inexpensive production of custom 3D printed equipment for large-volume fluorescence microscopy. International journal of pharmaceutics. 2015;494(2):651-6.
29. Herbert MR, Ziegler DA, Deutsch CK, O'Brien LM, Kennedy DN, Filipek PA, et al. Brain asymmetries in autism and developmental language disorder: a nested whole-brain analysis. Brain : a journal of neurology. 2005;128(Pt 1):213-26.
30. Alexander AL, Lee JE, Lazar M, Field AS. Diffusion tensor imaging of the brain. Neurotherapeutics : the journal of the American Society for Experimental NeuroTherapeutics. 2007;4(3):316-29.
31. Okuyama T, Kitamura T, Roy DS, Itohara S, Tonegawa S. Ventral CA1 neurons store social memory. Science. 2016;353(6307):1536-41.
32. Pitkanen A, Pikkarainen M, Nurminen N, Ylinen A. Reciprocal connections between the amygdala and the hippocampal formation, perirhinal cortex, and postrhinal cortex in rat. A review. Annals of the New York Academy of Sciences. 2000;911:369-91.
33. Cavada C, Company T, Tejedor J, Cruz-Rizzolo RJ, Reinoso-Suarez F. The anatomical connections of the macaque monkey orbitofrontal cortex. A review. Cerebral cortex. 2000;10(3):220-42.
34. Abrams DA, Lynch CJ, Cheng KM, Phillips J, Supekar K, Ryali S, et al. Underconnectivity between voice-selective cortex and reward circuitry in children with autism. Proceedings of the National Academy of Sciences of the United States of America. 2013;110(29):12060-5.
35. Murphy ER, Foss-Feig J, Kenworthy L, Gaillard WD, Vaidya CJ. Atypical Functional Connectivity of the Amygdala in Childhood Autism Spectrum Disorders during Spontaneous Attention to Eye-Gaze. Autism research and treatment. 2012;2012:652408.
36. Rutishauser U, Tudusciuc O, Wang S, Mamelak AN, Ross IB, Adolphs R. Single-neuron correlates of atypical face processing in autism. Neuron. 2013;80(4):887-99.
37. Sundaram SK, Kumar A, Makki MI, Behen ME, Chugani HT, Chugani DC. Diffusion tensor imaging of frontal lobe in autism spectrum disorder. Cerebral cortex. 2008;18(11):2659-65.
38. Fellgiebel A, Wille P, Muller MJ, Winterer G, Scheurich A, Vucurevic G, et al. Ultrastructural hippocampal and white matter alterations in mild cognitive impairment: a diffusion tensor imaging study. Dementia and geriatric cognitive disorders. 2004;18(1):101-8.
39. Stebbins GT, Murphy CM. Diffusion tensor imaging in Alzheimer's disease and mild cognitive impairment. Behavioural neurology. 2009;21(1):39-49.
40. Carlesimo GA, Cherubini A, Caltagirone C, Spalletta G. Hippocampal mean diffusivity and memory in healthy elderly individuals: a cross-sectional study. Neurology. 2010;74(3):194-200.
41. Ameis SH, Fan J, Rockel C, Voineskos AN, Lobaugh NJ, Soorya L, et al. Impaired structural connectivity of socio-emotional circuits in autism spectrum disorders: a diffusion tensor imaging study. PloS one. 2011;6(11):e28044.
42. Shukla DK, Keehn B, Muller RA. Tract-specific analyses of diffusion tensor imaging show widespread white matter compromise in autism spectrum disorder. Journal of child psychology and psychiatry, and allied disciplines. 2011;52(3):286-95.
43. Jou RJ, Jackowski AP, Papademetris X, Rajeevan N, Staib LH, Volkmar FR. Diffusion tensor imaging in autism spectrum disorders: preliminary evidence of

714 abnormal neural connectivity. The Australian and New Zealand journal of psychiatry.
715 2011;45(2):153-62.
716 44. Conturo TE, Williams DL, Smith CD, Gultepe E, Akbudak E, Minshew NJ.
717 Neuronal fiber pathway abnormalities in autism: an initial MRI diffusion tensor
718 tracking study of hippocampo-fusiform and amygdalo-fusiform pathways. Journal of
719 the International Neuropsychological Society : JINS. 2008;14(6):933-46.
720 45. Missler M, Zhang W, Rohlmann A, Kattenstroth G, Hammer RE, Gottmann
721 K, et al. Alpha-neurexins couple Ca2+ channels to synaptic vesicle exocytosis.
722 Nature. 2003;423(6943):939-48.
723 46. Alba-Ferrara LM, de Erausquin GA. What does anisotropy measure? Insights
724 from increased and decreased anisotropy in selective fiber tracts in schizophrenia.
725 Frontiers in integrative neuroscience. 2013;7:9.
726 47. Minshew NJ, Williams DL. The new neurobiology of autism: cortex,
727 connectivity, and neuronal organization. Archives of neurology. 2007;64(7):945-50.
728 48. Andreae LC, Burrone J. Spontaneous Neurotransmitter Release Shapes
729 Dendritic Arbors via Long-Range Activation of NMDA Receptors. Cell reports. 2015.
730 49. Ye L, Allen WE, Thompson KR, Tian Q, Hsueh B, Ramakrishnan C, et al.
731 Wiring and Molecular Features of Prefrontal Ensembles Representing Distinct
732 Experiences. Cell. 2016;165(7):1776-88.
733 50. Jones DK. The effect of gradient sampling schemes on measures derived from
734 diffusion tensor MRI: a Monte Carlo study. Magnetic resonance in medicine.
735 2004;51(4):807-15.
736 51. Lebel C, Benner T, Beaulieu C. Six is enough? Comparison of diffusion
737 parameters measured using six or more diffusion-encoding gradient directions with
738 deterministic tractography. Magnetic resonance in medicine. 2012;68(2):474-83.
739 52. Hasan KM, Parker DL, Alexander AL. Comparison of gradient encoding
740 schemes for diffusion-tensor MRI. Journal of magnetic resonance imaging : JMRI.
741 2001;13(5):769-80.
742 53. Yao X, Yu T, Liang B, Xia T, Huang Q, Zhuang S. Effect of increasing
743 diffusion gradient direction number on diffusion tensor imaging fiber tracking in the
744 human brain. Korean journal of radiology. 2015;16(2):410-8.
745 54. Ni H, Kavcic V, Zhu T, Ekholm S, Zhong J. Effects of number of diffusion
746 gradient directions on derived diffusion tensor imaging indices in human brain. AJNR
747 American journal of neuroradiology. 2006;27(8):1776-81.
748

Figure Legends

Figure 1

Quantification of CLARITY imaging. **A** Sections of DTI-scanned brain were segmented at different Bregma levels for (i) the orbitofrontal cortex, (ii) the anterior hippocampus and amygdala, (iii) the mid hippocampus and posterior amygdala and (iv) the posterior hippocampus. **B-D** DTI-scanned brains were computed for tracts. Tissue from wild-type and *Nrxn2α* KO mice were cleared and stained for neurofilament and DAPI (**E**). **F** Automated MATLAB scripts were used to segment the DAPI (blue) and neurofilament (purple) channels such that cell density and axonal density and orientation could be calculated. **G** is representative of a CLARITY-derived 3D stacked image of a DAPI and neurofilament of a region of interest, with **H** being the corresponding segmented image. Scale bar: 100 μm.

Figure 2

Deletion of *Nrxn2α* reduces amygdala fractional anisotropy (FA) but not apparent diffusion coefficient (ADC). DTI images of the amygdala was segmented at two regions; anterior (Bregma -1.94 mm) and posterior (Bregma -2.46 mm). FA of the whole amygdala structure was significantly reduced in the posterior (**B**) but not (**A**) region. FA was also significantly reduced in the anterior basolateral amygdala (BLA) (**C**). However, ADC was similar between the genotypes in the anterior (**D**), posterior (**E**) and BLA (**F**). **=P<0.01, *=P<0.05. Error bars represent s.e.m. Wild-type n=6, *Nrxn2α* KO n=6.

Figure 3

774 *Nrxn2α* KO mice have increased apparent diffusion coefficient (ADC) and
775 axial (AD) and radial diffusivity (RD) in the orbitofrontal cortex (OFC) and the
776 anterior cingulate cortex (ACC). Although reduced, there was no significant
777 difference between wild-types and *Nrxn2α* KO mice for FA in the OFC (**A**) and
778 ACC (**C**), but ADC was significantly increased in *Nrxn2α* KO mice in both
779 prefrontal regions (**B** and **D**). The OFC has significantly increased AD and RD
780 (**E-F**), whereas only RD was increased in the ACC (**G-H**). ***=P=0.0005,
781 ***=P<0.001, **=P<0.01, *=P<0.05. Error bars represent s.e.m. Wild-type n=6,
782 *Nrxn2α* KO n=6.
783
784 **Figure 4**
785 Tractographic analysis of amygdala-hippocampus and amygdala-orbitofrontal
786 cortex (OFC) connectivity. Amygdala-hippocampal connections are
787 characterised by greater right hemisphere axial diffusivity (AD) *Nrxn2α* KO
788 mice (**A**) but not radial diffusivity (RD) (**B**). Specific to the BLA, connections to
789 the anterior hippocampus (**C**) and posterior hippocampus (**D**) have greater
790 right hemisphere AD. Although the amygdala-OFC connection was similar
791 between the genotypes for AD (**E**), *Nrxn2α* KO mice had significantly
792 increased RD (**F**). *=P<0.05, ***=P<0.001. Error bars represent s.e.m. Wild-
793 type n=6, Nrxn2α KO n=6.
794
795 **Figure 5**
796 CLARITY reveals differences in axonal alignment and fibre density in *Nrxn2α*
797 KO mice. (**A-C**) Representative images of the CLARITY-treated brain, with
798 ROI defined for the anterior cingulate cortex (ACC), orbitofrontal cortex

(OFC), basomedial amygdala (BMA) and basolateral amygdala (BLA). For the ACC, the axonal alignment (**D**) and axon density (**E**) were significantly altered in KO mice, but cell density was unaltered (**F**). Within the medial OFC, only axonal alignment was significantly altered in KOs (**G**), with axon density (**H**) and cell density (**I**) being similar. For the BMA, both the axonal alignment (**J**) and axon density (**K**) were significantly increased, whilst cell density was unaltered (**L**). *=P<0.05, **=P<0.01. Error bars represent s.e.m. Wild-type n=6, *Nrxn2α* KO n=6.

Figure 1

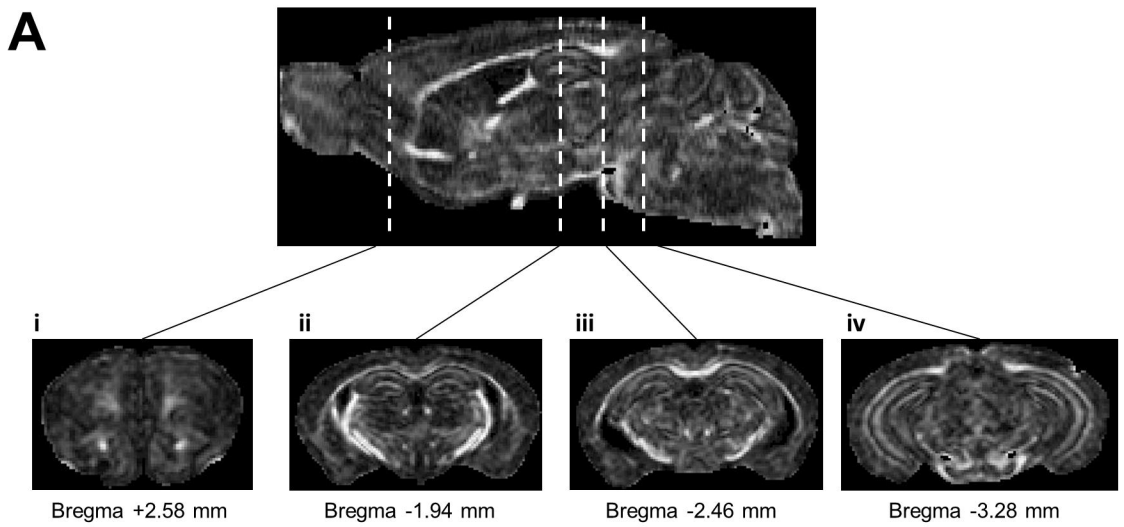

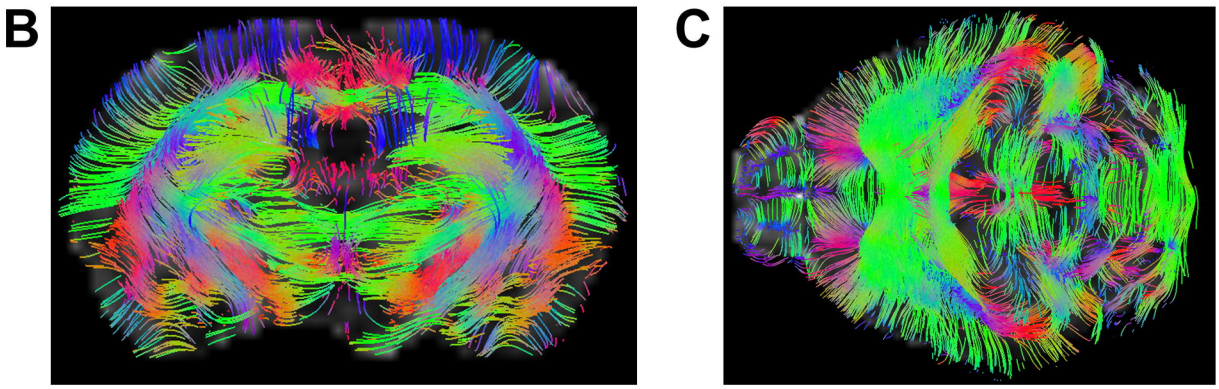

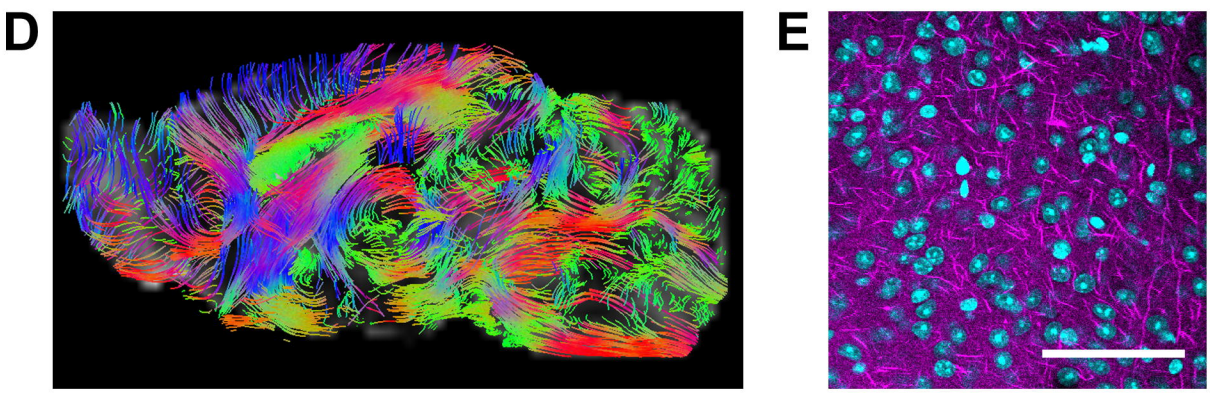

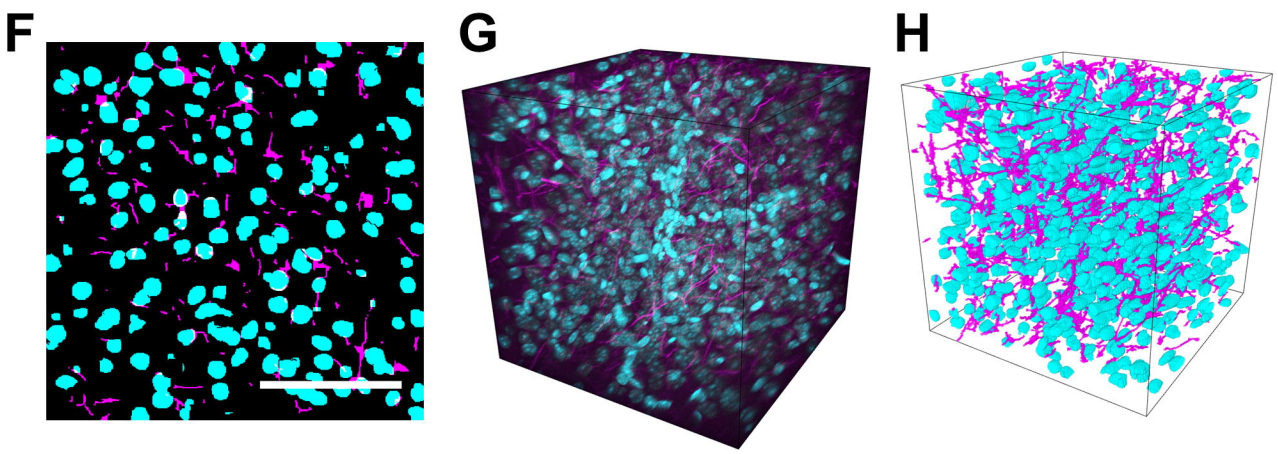

Figure 2

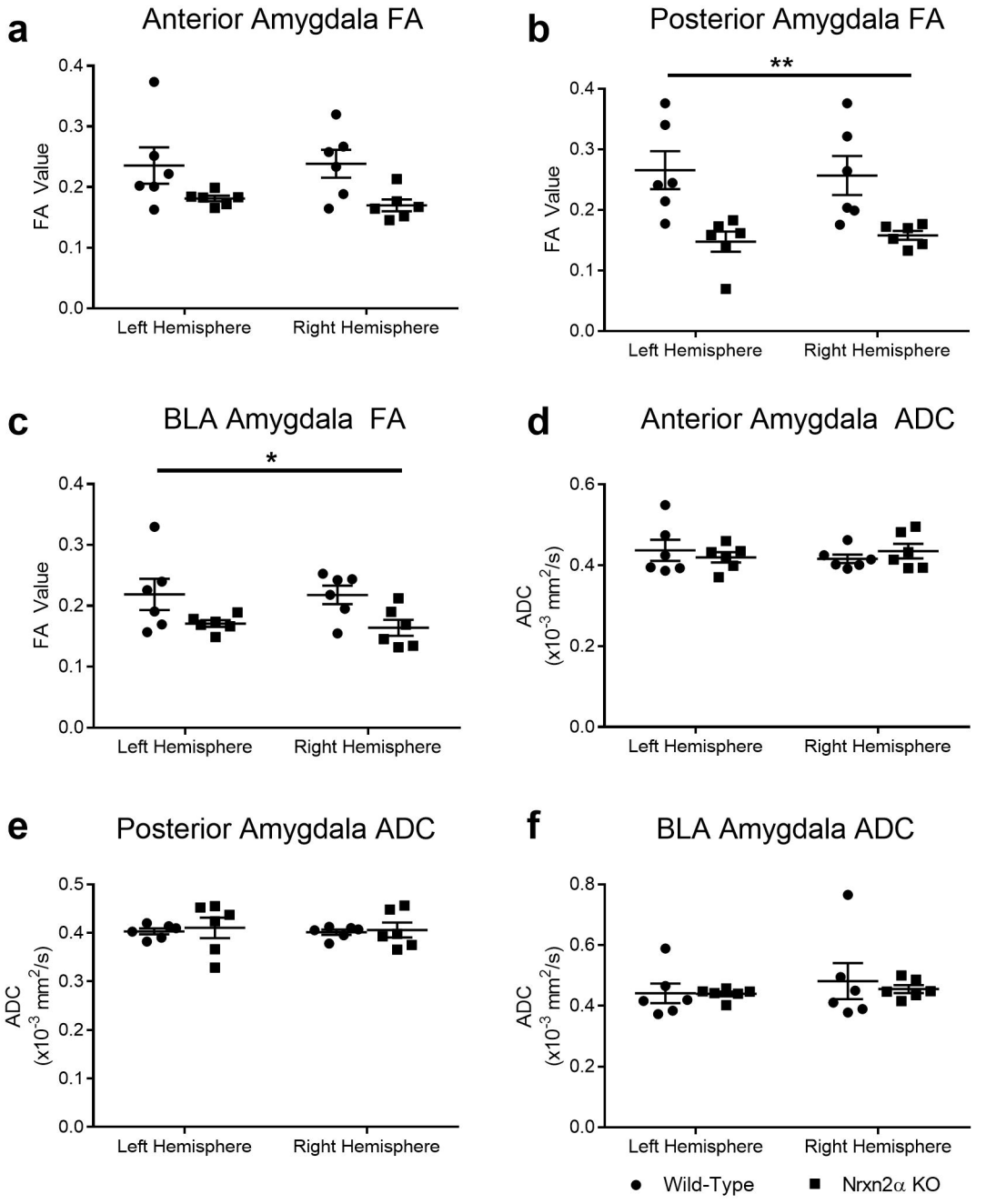
a
Anterior Amygdala FA
FA Value
0.4
0.3
0.2
0.1
0.0
Left Hemisphere
Right Hemisphere
b
Posterior Amygdala FA
**
FA Value
0.4
0.3
0.2
0.1
0.0
Left Hemisphere
Right Hemisphere
c
BLA Amygdala FA
*
FA Value
0.4
0.3
0.2
0.1
0.0
Left Hemisphere
Right Hemisphere
d
Anterior Amygdala ADC
ADC
(x10-3 mm2/s)
0.6
0.4
0.2
0.0
Left Hemisphere
Right Hemisphere
e
Posterior Amygdala ADC
ADC
(x10-3 mm2/s)
0.5
0.4
0.3
0.2
0.1
0.0
Left Hemisphere
Right Hemisphere
f
BLA Amygdala ADC
ADC
(x10-3 mm2/s)
0.8
0.6
0.4
0.2
0.0
Left Hemisphere
Right Hemisphere
Wild-Type
Nrxn2α KO

Figure 3

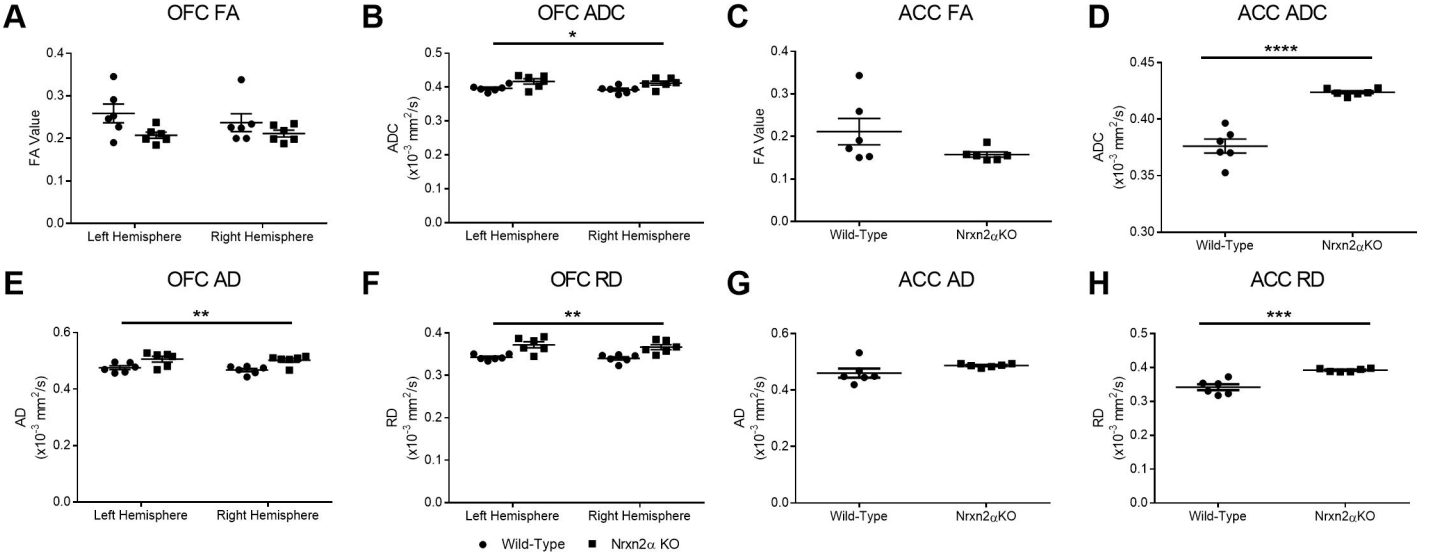
A
OFC FA
FA Value
0.4
0.3
0.2
0.1
0.0
Left Hemisphere
Right Hemisphere
B
OFC ADC
*
ADC
(x10-3 mm2/s)
0.5
0.4
0.3
0.2
0.1
0.0
Left Hemisphere
Right Hemisphere
C
ACC FA
FA Value
0.4
0.3
0.2
0.1
0.0
Wild-Type
Nrxn2αKO
D
ACC ADC
****
ADC
(x10-3 mm2/s)
0.45
0.40
0.35
0.30
Wild-Type
Nrxn2αKO
E
OFC AD
**
AD
(x10-3 mm2/s)
0.6
0.4
0.2
0.0
Left Hemisphere
Right Hemisphere
F
OFC RD
**
RD
(x10-3 mm2/s)
0.4
0.3
0.2
0.1
0.0
Left Hemisphere
Right Hemisphere
Wild-Type
Nrxn2α KO
G
ACC AD
AD
(x10-3 mm2/s)
0.6
0.4
0.2
0.0
Wild-Type
Nrxn2αKO
H
ACC RD
***
RD
(x10-3 mm2/s)
0.5
0.4
0.3
0.2
0.1
0.0
Wild-Type
Nrxn2αKO

Figure 4

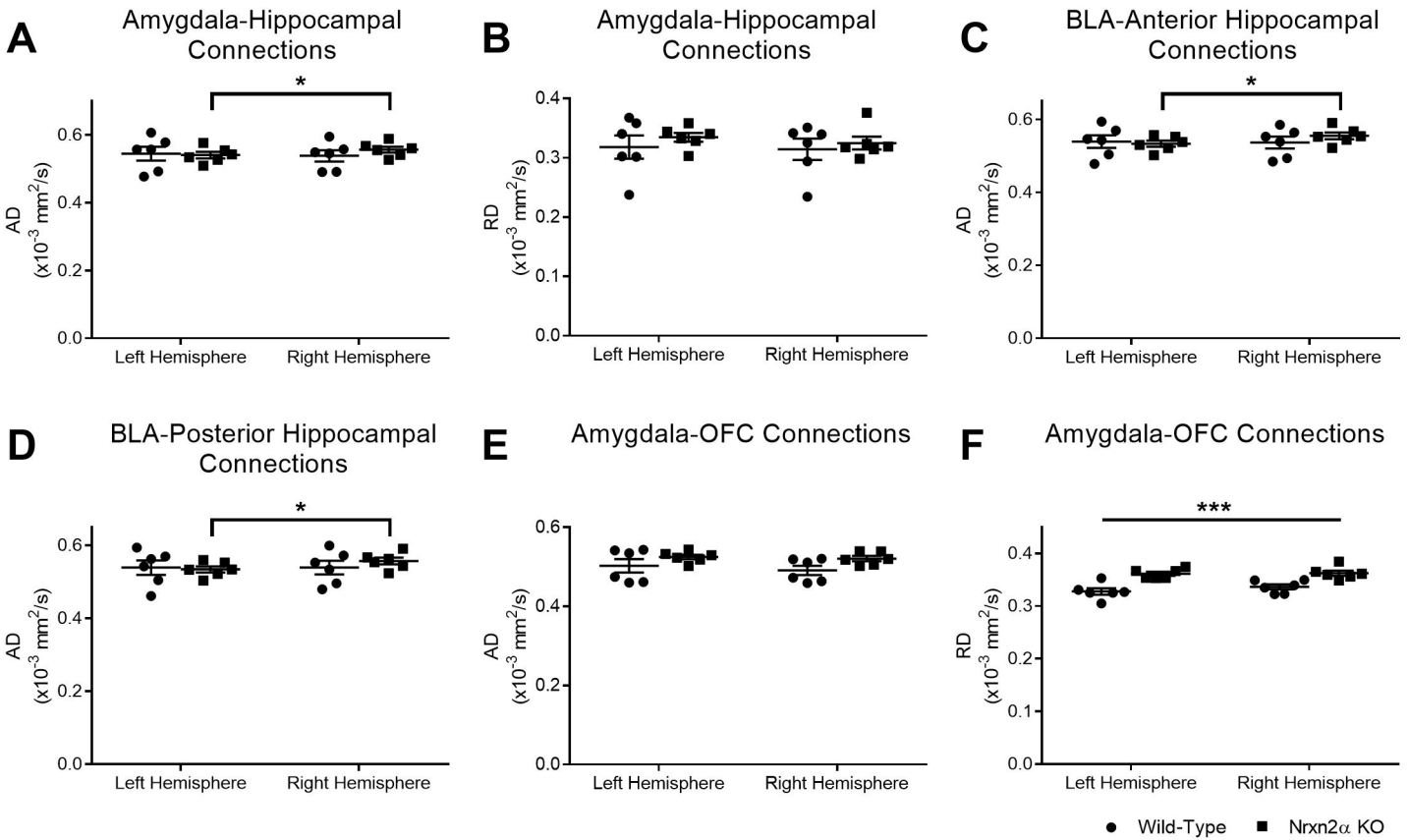
A
Amygdala-Hippocampal Connections
*
AD (x10-3 mm2/s)
0.0
0.2
0.4
0.6
Left Hemisphere
Right Hemisphere
B
Amygdala-Hippocampal Connections
RD (x10-3 mm2/s)
0.0
0.1
0.2
0.3
0.4
Left Hemisphere
Right Hemisphere
C
BLA-Anterior Hippocampal Connections
*
AD (x10-3 mm2/s)
0.0
0.2
0.4
0.6
Left Hemisphere
Right Hemisphere
D
BLA-Posterior Hippocampal Connections
*
AD (x10-3 mm2/s)
0.0
0.2
0.4
0.6
Left Hemisphere
Right Hemisphere
E
Amygdala-OFC Connections
AD (x10-3 mm2/s)
0.0
0.2
0.4
0.6
Left Hemisphere
Right Hemisphere
F
Amygdala-OFC Connections
***
RD (x10-3 mm2/s)
0.0
0.1
0.2
0.3
0.4
Left Hemisphere
Right Hemisphere
Wild-Type
Nrxn2α KO

Figure 5